Journal of Materials Chemistry C

PAPER

View Article Online
View Journal | View Issue

Cite this: J. Mater. Chem. C, 2014, 2, 4289

Synthesis and properties of indigo based donor–acceptor conjugated polymers†

Chang Guo, Bin Sun, Jesse Quinn, Zhuangqing Yan and Yuning Li*

Received 18th November 2013
Accepted 23rd February 2014

DOI: 10.1039/c3tc32276a

www.rsc.org/MaterialsC

Indigo is for the first time used as a building block to construct polymer semiconductors for organic thin film transistors (OTFTs). Two donor–acceptor polymers using indigo as the acceptor and bithiophene as the donor are synthesized *via* Stille coupling polymerization. Two types of acyl groups, 2-hexldecanoyl (for polymer **P1**) and 2-octyldodecanoyl (for polymer **P2**), are utilized as solubilizing side chains. These polymers possess very deep highest-occupied molecular orbital (HOMO) and lowest unoccupied molecular orbital (LUMO) energy levels, due to the strong electron accepting capability of the indigo moiety. In OTFT devices, characteristic n-type semiconductor performance with electron mobility of up to $\sim 10^{-3}$ cm^2 V^{-1} s^{-1} is observed.

Introduction

Conjugated polymers comprising alternating electron donor (D) and acceptor (A) moieties in the backbone have been receiving much attention recently as active semiconductors for organic thin film transistors (OTFTs)[1,2] and organic photovoltaics (OPVs).[3–12] Intramolecular charge transfer between the donor and acceptor moieties allows these polymers to absorb visible and even near infrared portions of the sun light, making many D–A polymers good candidate donor materials for OPVs.[13–15] On the other hand, it has been found that the donor and acceptor units on the adjacent polymer chains in the solid state could effectively strengthen the intermolecular interactions, making the polymer chains tightly packed along the π–π stacking direction in comparison to the polymers with only donor units.[16–18] The shortened π–π stacking distance could greatly facilitate charge carrier hopping between polymer chains, resulting in very high carrier mobility of over 1 cm^2 V^{-1} s^{-1} for some D–A polymers.[1,2] Although the electron donor units play an important role for achieving such high mobility values, the electron acceptor building blocks are considered to be the determining factor. The majority of high mobility polymers are based on a few types of electron acceptors such as diketopyrrolopyrrole (DPP)[17,19–23] and isoindigo (IID).[24–27] To bring the charge transport performance beyond the current level, new acceptor building blocks need to be explored and developed.

A structural isomer of isoindigo, the indigo (ID) blue dye has been widely used since as early as 1600 BC (Fig. 1).[28–30] The non-substituted indigo can form intramolecular hydrogen bonding between the oxygen and the hydrogen atoms of the two 1*H*-indol-3-one units, resulting in a highly coplanar geometry of the indigo molecule.[31–34] Indigo has a much longer wavelength of absorption maximum (λ_{max} = 600–610 nm)[35,36] than that of isoindigo (λ_{max} = 520–540 nm)[37–40] in solutions, indicating the more effective conjugation of the former. Recently, indigo and its derivative, tyrian purple (6,6′-dibromoindigo), have been used as semiconducting channel materials in OTFTs.[28,41–43] The devices based on these compounds showed ambipolar charge transport characteristics with a hole mobility of up to 0.40 cm^2 V^{-1} s^{-1}. According to a recent report,[44] the hole and electron

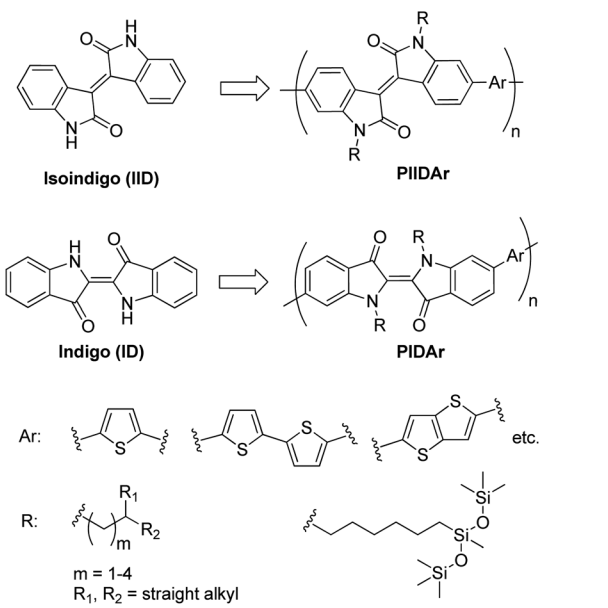

Fig. 1 Structures of isoindigo (IID) and indigo (ID) and their polymers.

Department of Chemical Engineering and Waterloo Institute for Nanotechnology (WIN), University of Waterloo, 200 University Ave West ON, Waterloo, Canada, N2L 3G1. E-mail: yuning.li@uwaterloo.ca; Fax: +1-519-888-4347; Tel: +1-519-888-4567 ext. 31105

† Electronic supplementary information (ESI) available: Additional computer simulation data, NMR, DSC, and TGA. See DOI: 10.1039/c3tc32276a

mobilities of indigo and tyrian purple calculated based on the Marcus's method[45] are very similar to those of isoindigo. The high mobility values both experimentally achieved and theoretically predicted for indigo and its derivatives suggest that indigo might be another promising electron acceptor building block for D–A polymers for organic electronics. In this study, we report the synthesis and properties of two polymers comprising indigo (acceptor) and bithiophene (donor), which are, to the best of our knowledge, the first D–A polymers based on indigo.

Results and discussion

D–A polymers based on 6,6′-isoindigo and bithiophene, PIIDBT (Ar = bithiophene in Fig. 1), were reported to show very high charge transport performance in OTFTs with a hole mobility of up to 3.62 $cm^2 V^{-1} s^{-1}$.[27] The closest structural analogue of their indigo based polymers would be PIDBT (Ar = bithiophene) as shown in Fig. 1, where the indigo unit is connected at the 6 and 6′ positions with the neighbouring thiophene units. In this study, we chose 6,6′-dibromoindigo or tyrian purple (**1**), as the starting material to construct PIDBT polymers. Compound **1** was readily prepared with ~70% yield in one step by using a literature method (Scheme 1).[46] Substitution at the nitrogen atoms with suitable side chains such as alkyl groups can improve the solubility of the resulting substituted indigo molecules and the final polymers. However, our attempts to substitute compound **1** using an alkyl bromide such as 2-octadodecyl bromide in the presence of a base (*e.g.*, K_2CO_3 and NaH) only led to mono-alkylated products. Similar observations were also reported for the substitution of indigo.[47] Finally we found that the nitrogen atoms of **1** could be readily substituted with acyl groups by using the chemistry we used for DPP.[48] Because most D–A polymers have very strong intermolecular interactions, they generally have poor solubility in organic solvents. Therefore, we used long branched side chains, 2-hexldecanoyl and 2-octyldodecanoyl groups, to substitute the nitrogen atoms of compound **1**, resulting in **2a** and **2b** with 34% and 39% yields, respectively (Scheme 1). It has been reported that acyl substituted indigo compounds undergo photoisomerization from the stable *trans*-isomers to the less stable *cis*-isomers.[49,50]

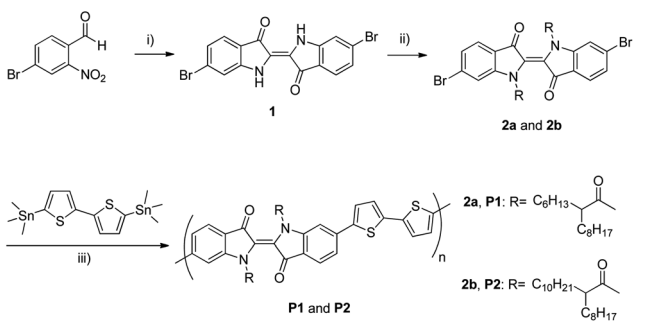

Scheme 1 Synthetic route for indigo monomers **2a** and **2b** and polymers **P1** and **P2**: (i) NaOH/acetone/room temp.; (ii) (a) NaH/NMP/room temp., (b) RCOCl/room temp.; (iii) $Pd_2(dba)_3$/P(*o*-tolyl)$_3$/chlorobenzene/90 °C.

^{1}H NMR spectra of **2a** and **2b** indeed indicated the presence of ~85% of the *trans*-isomer and ~15% of the *cis*-isomer when the solutions were prepared under ambient light. Two PIDBT polymers, **P1** and **P2**, were synthesized *via* Stille coupling polymerizations of **2a** and **2b**, respectively, with 2,5′-bis(trimethyl) stannylbithiophene using $Pd_2(dba)_3$/P(*o*-toyl)$_3$ as a catalyst system in chlorobenzene at 90 °C. Polymers were purified with a Sohxlet extraction apparatus using sequentially acetone, hexane and chloroform, and then the remaining solid was heated in 1,1,2,2-tetrachloroethane (TCE) at 130 °C in a flask. Acetone and hexane were used to remove the catalyst residues and oligomers, respectively, chloroform and TCE were used to dissolve the higher molecular weight polymer fraction. **P1** showed poor solubility; it is essentially insoluble in chloroform and only 15% of the polymer was dissolved by hot TCE. The very poor solubility of **P1** indicates the very strong intermolecular D–A interactions of this polymer. **P2** with longer 2-octyldodecanoyl side chains showed improved solubility with 13% dissolved in chloroform and 59% dissolved in TCE, but ~28% of the polymer still remained insoluble. The molecular weights of these two polymers were determined by using gel permeation chromatography (GPC) with chlorobenzene as the eluent and polystyrene as the standards at a column temperature of 40 °C. The number average molecular weight (M_n) of **P1** dissolved in TCE is 13.5 kDa with a polydispersity index (PDI) of 3.50. The fraction of **P2** extracted with chloroform has a slightly lower M_n of 12.4 kDa. However, the weight average molecular weight (M_w) of **P2** is 131.4 kDa, which is much higher than that of **P1** (47.3 kDa), resulting in a very broad PDI of 10.6. The molecular weight of **P2** dissolved in TCE could not be measured because of its very poor solubility in chlorobenzene used for the GPC measurements at 40 °C. However, we can reasonably assume that the molecular weight of **P2** in the TCE fraction should be higher than that of **P1**. The results used for the following discussions were obtained using the fractions of **P1** and **P2** dissolved in TCE.

The thermal properties of polymers were characterized by using thermogravimetric analysis (TGA) and differential scanning colorimetry (DSC). **P1** and **P2** had 5% weight losses at 160 °C and 220 °C, respectively, indicating that these polymers are quite thermally labile. DSC diagrams clearly showed an exothermic peak at 258 °C in the first heating scan for both polymers. These results are reminiscent of the behaviour of a DPP based polymer that also has acyl (2-octadodecanoyl) substituents at the nitrogen atoms, where the 2-octadodecanoyl substituents were found to be thermally unstable and the polymer started to loose side chains at ~180 °C.[48] Therefore the thermal instability observed for **P1** and **P2** is most likely caused by the thermally labile acyl groups.

Unlike the substituted isoindigo, where the substituents at the nitrogen atoms are distant from their neighbouring indol-2-one rings, substitution of indigo at the nitrogen atoms might cause twisting of the indigo moiety because the acyl side chains are very close to the C=O groups of the neighbouring indol-3-one rings. An acetyl-substituted dimer compound, IDCOMe-BT-IDCOMe-BT, was simulated by performing density functional theory (DFT) calculations using Gaussian 09W[51,52] to determine the influence of acyl substitution on the coplanarity of the

indigo moiety. As shown in Fig. 2, the dihedral angle between the two indol-3-one moieties in the acetyl-substituted indigo unit (φ_1) is ~23°. On the other hand, the dihedral angle between the two indol-2-one moieties in the methyl-substituted IID unit (φ_1) of an analogous dimer, IIDMe-BT-IIDMe-BT, is only ~11° (similar results were reported using the same simulation protocols).[53,54] We also simulated the methyl-substituted indigo dimer, IDMe-BT-IDMe-BT, the dihedral angle φ_1 increased further to 29° (see ESI†). Additionally, the dihedral angles between the indigo and thiophene ($\varphi_2 = 24°$) and between two thiophene units ($\varphi_3 = 15°$) are also greater than the respective dihedral angles of its isoindigo dimer ($\varphi_2 = 20°$; $\varphi_3 = 5°$). These results indicate that the acyl-substituted PIDBT (**P1** or **P2**) has a more twisted backbone than that of the alkyl-substituted PIIDBT.

Compound **1** had a λ_{max} at 586 nm in TCE (Fig. 3a), which agrees with the reported value of 585 nm.[55] The acyl-substituted **2a** and **2b** had a λ_{max} at 576 nm in TCE solutions. The blue shift of ~10 nm λ_{max} for **2a** and **2b** with respect to compound **1** is likely to be the result of the twisted indigo moiety caused by the acyl groups. Polymers **P1** and **P2** had λ_{max} values at 527 nm and 572 nm, respectively, in TCE solutions, and 607 nm and 620 nm, respectively, in the solid state (as-spun films) as can be seen in Fig. 3b. The longer absorption wavelengths of **P2** than those of **P1** are considered to be due to the higher molecular weight and thus the longer effective conjugation length of **P2**. By comparing **P2** with its isoindigo analogue, PIIDBT-20 (Ar = bithiophene and R = 2-octyldodecyl in Fig. 1), which had a λ_{max} value at 706 nm in solution and 701 nm in film,[27] the λ_{max} values of **P2** both in solution and in the solid state blue shifted notably. This suggests that **P2** has a shorter main chain conjugation length

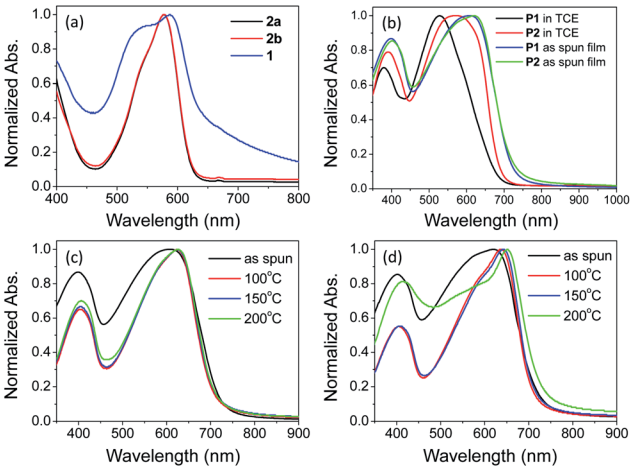

Fig. 3 UV-vis absorption spectra of (a) **1**, **2a** and **2b** in TCE solutions; (b) **P1** and **P2** in TCE solutions and in thin films; (c) **P1** and (d) **P2** thin films on glass substrates annealed at different temperatures.

than that of PIIDBT-20. As noted earlier, small molecular indigoids have longer absorption wavelengths and are structurally more conjugated than their isoindigo counterparts. The observed reduction in conjugation for **P2** compared with PIIDBT-20 might be accounted for by the substitution of indigo at the nitrogen atoms with the acyl groups, leading to a more twisted polymer backbone and reduced main chain conjugation. Another possible reason might be due to the presence of some *cis*-indigo units on the polymer backbone, which might also cause serious twisting and less ordered packing of the polymer chains in the solid state. It was reported that the λ_{max} of

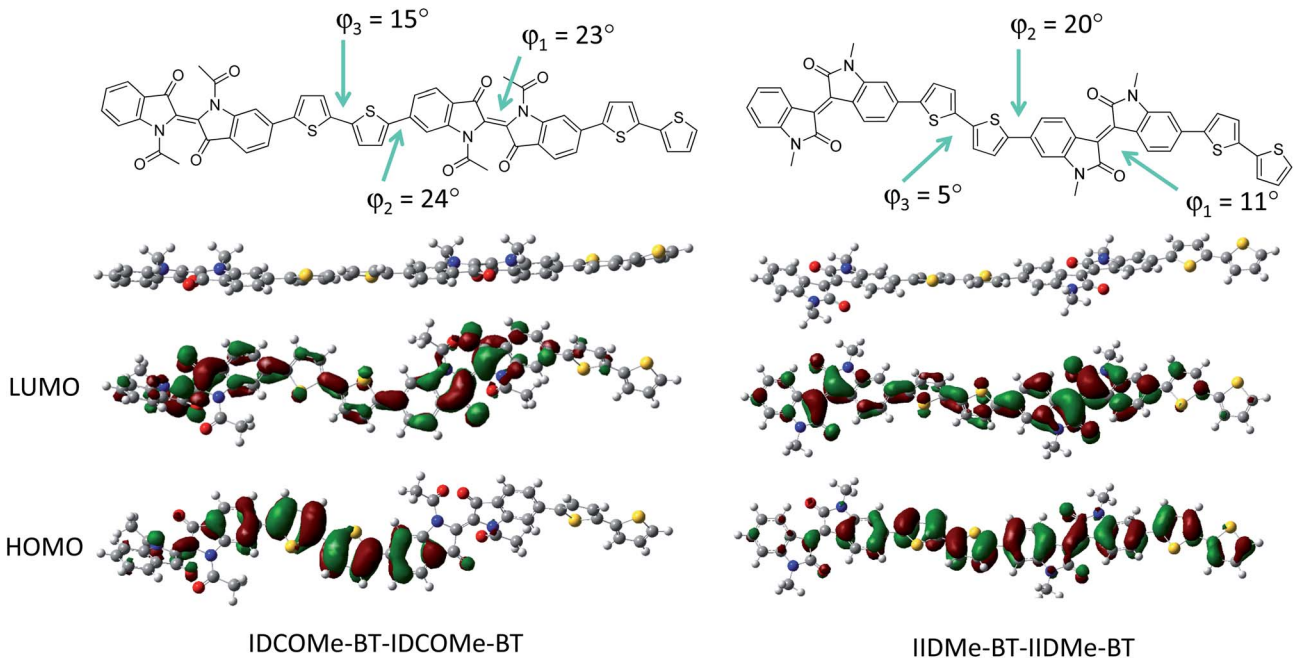

Fig. 2 The chemical structure, geometry, LUMO orbital, and HOMO orbital of two model dimers IDCOMe-BT-IDCOMe-BT and IIDMe-BT-IIDMe-BT, which correspond to acyl-substituted PIDBT (**P1** or **P2**) and alkyl-substituted PIIDBT,[27] respectively, obtained by performing DFT calculations with the B3LYP 6-31G* basis set.

cis-IDCOMe is 438 nm (in benzene), which is significantly blue shifted compared with that of *trans*-IDCOMe (562 nm).[49]

When the thin films were thermally annealed, both polymers showed apparent red shits in their UV-Vis spectra (Fig. 3c and d). The λ_{max} of the 100 °C-annealed **P1** thin film red shifted to 626 nm. Further increasing the annealing temperature to 150 and 200 °C did not change the λ_{max} of **P1** thin films. For the **P2** thin films, the λ_{max} red shifted progressively to 639 and 643 nm as the annealing temperature increased to 100 and 150 °C, respectively. Thermal annealing would increase the chain ordering as manifested by the following XRD results and might also transform the *cis*-indigo to the *trans*-indigo,[56] leading to more extended π-conjugation of the polymer backbone. The 200 °C-annealed **P2** sample had a dramatically different absorption profile and a further red-shifted λ_{max} at 651 nm. This is most likely due to the removal of acyl side chains at such a high annealing temperature, revealed by the TGA data. The indigo units without substitution at the nitrogen atoms are almost coplanar (see ESI†).

The energy levels of the two polymers were determined by cyclic voltammetry (CV) in the solid thin film state using ferrocene as the standard that has a HOMO level of −4.8 eV.[57] **P2** showed reversible oxidative and reductive cycles (Fig. 4). The HOMO/LUMO levels of **P2** were calculated by using the onset oxidative/reductive potentials to be −5.78 eV and −4.02 eV, respectively. The band gap of 1.68 eV determined by CV is close to the optical band gap of 1.74 eV calculated from the onset absorption wavelength of the as-spun film. The HOMO/LUMO levels of **P2** obtained by CV are slightly lower than those of PIIDBT-20 ($E_{HOMO} = -5.70$ eV and $E_{LUMO} = -3.70$ eV relative to the ferrocene standard).[27] The HOMO and LUMO levels of the as-spun **P1** film were determined to be −5.69 eV and −4.00 eV, respectively.

The crystallinity of polymers was studied by using X-ray diffractometry (XRD) of polymer thin films spin coated on SiO_2/Si substrates. The **P1** film annealed at 100 °C exhibited a weak primary peak at $2\theta = 4.86°$, which corresponds to a *d*-spacing distance of 1.82 nm (Fig. 5). When the annealing temperature was increased to 150 °C, the primary peak shifted slightly to $2\theta = 4.81°$ (*d*-spacing = 1.84 nm). Once the annealing temperature was raised to 200 °C, the primary peak disappeared. This is due to the loss of side chains at such a high temperature as corroborated by the thermal analysis data. The 100 °C-annealed **P2** film had a very weak primary peak at $2\theta = 4.30°$, corresponding to a *d*-spacing distance of 2.05 nm. Increasing the annealing temperature to 150 °C improved the crystallinity of the **P2** film significantly, manifested by the much intensified peak at $2\theta = 4.38°$ (*d*-spacing = 2.02 nm). Further increasing the annealing temperature to 200 °C, the intensity of the primary peak decreased and the *d*-spacing further decreased to 1.92 nm ($2\theta = 4.58°$), again due to the loss of the side chains. Since the XRD diagrams of the crystalline polymer thin films only showed the primary peaks, the polymer chains of **P1** and **P2** most likely adopted a layer-by-layer lamellar packing motif,[58] a commonly observed crystal structure for most π-conjugated polymers in thin films.[1,2,59] The atomic force microscopic (AFM) images of the 100 °C- and 150 °C-annealed **P1** thin films contain large grains (Fig. 6). The 200 °C-annealed **P1** thin film became more uniform, probably due to the removal of the side chains. On the other hand, all of the **P2** thin films are very smooth and the surface morphology was not much influenced by thermal annealing.

P1 and **P2** were tested as channel semiconductors in top-gate, bottom-contact OTFTs. Heavily n-doped Si/SiO_2 wafer patterned with gold source and drain electrode pairs (with a channel length of 30 μm and a channel width of 1 mm) was used as the substrate. A polymer solution in TCE was spin coated on the substrate to form a polymer thin film (~30–50 nm), which was annealed at 100, 150, or 200 °C on a hot plate, followed by spin coating a CYTOP layer (~500 nm) as the gate dielectric in a glove box under nitrogen. The capacitance per unit area (C_i) of the dielectric layer (3.2 nF cm^{-2}) was determined from a metal–insulator–metal (MIM) structure. The devices were characterized in ambient conditions in the absence of light. Devices with **P1** or **P2** thin films annealed at 100 °C showed no field effect performance. Devices based on **P1** thin films annealed at 150 °C showed characteristic electron transport behaviour with a mobility as high as 6.6×10^{-4} cm^2 V^{-1} s^{-1} (current on-to-off ratios of $\sim 10^4$) (Fig. 7a and b). Devices based on **P2** thin films annealed at 150 °C also exhibited electron transport performance with improved mobility of up to 1.1×10^{-3} cm^2 V^{-1} s^{-1} (on-to-off ratios of $\sim 10^4$) (Fig. 7c and d). No hole transport was observed for both polymers, which is presumably due to the

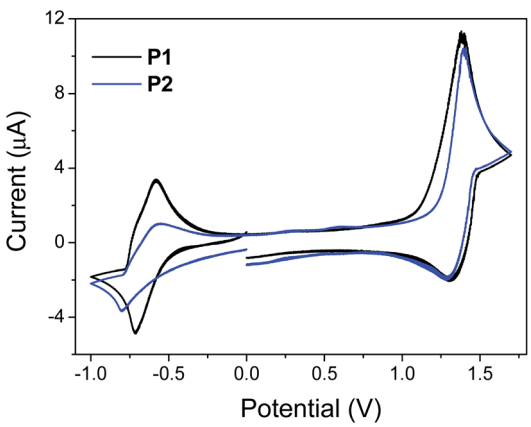

Fig. 4 Cyclic voltammograms of as-spun **P1** and **P2** thin films measured in anhydrous CH_3CN solution using Bu_4NPF_6 as the electrolyte.

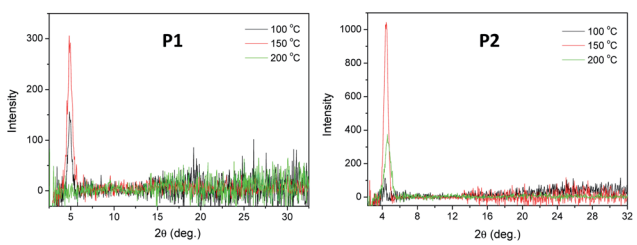

Fig. 5 XRD diagrams obtained from spin-coated **P1** and **P2** thin film on silicon substrates annealed at 100, 150 and 200 °C.

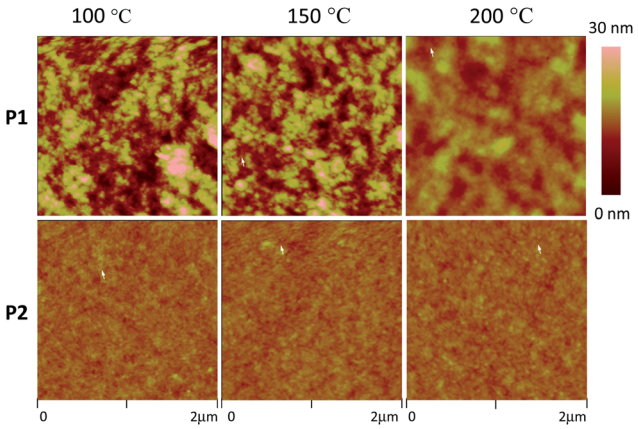

Fig. 6 AFM images (2 μm × 2 μm) of **P1** and **P2** thin films (~50–60 nm) spin coated on Si/SiO_2 substrate annealed at 100, 150 and 200 °C under nitrogen.

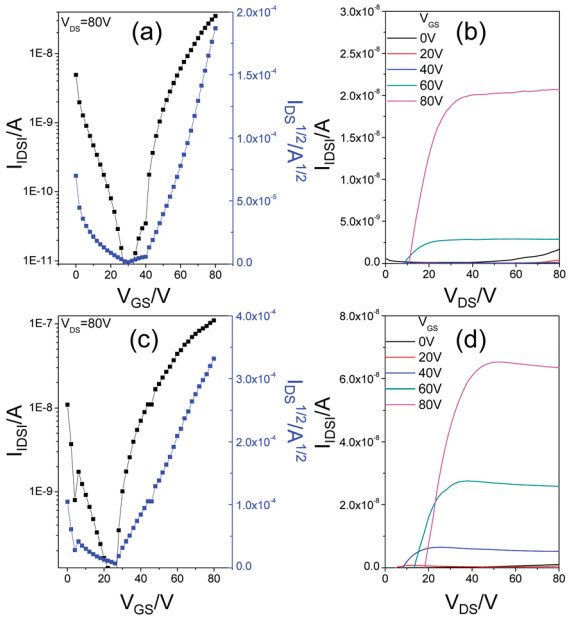

Fig. 7 Transfer and output curves of OTFT devices with **P1** (a and b) and **P2** (c and d) thin films annealed at 150 °C for 20 min. Device dimensions: channel width (W) = 1 mm; channel length (L) = 30 μm.

large hole injection barrier between their low-lying HOMO levels and the work function of gold (~4.7–5.1 eV).[60,61] The much lower mobility values observed for **P1** and **P2** in comparison to their isoindigo counterpart, PIIDBT-20, and small molecular indigoids is considered to originate from its poor main chain conjugation which is caused by the backbone twisting as discussed previously. The significantly poorer crystallinity (molecular ordering) of **P1** and **P2**, which originates from the main chain twisting and the possible existence of *cis*-isomers, also accounts for their low mobility values. Further increasing the annealing temperature to 200 °C resulted in the absence of field effect performance for both polymers, due to the deteriorated molecular ordering caused by thermal decomposition of the side chains. Substitution of the indigo units with more desirable side chains to minimize the steric effect and eliminate the *cis*-isomers is expected to improve the backbone coplanary and molecular organization for more efficient charge transport of the indigo based polymers.

Experimental

Materials and characterization

All chemicals were purchased from Sigma-Aldrich and were used without further purification. CYTOP (a perfluoronated amorphous resin solution) was purchased from AGC Chemicals. 6,6′-Dibromo-[2,2′-biindolinylidene]-3,3′-dione (**1**) was synthesized according to the literature.[46] NMR spectra were obtained on a Bruker DPX 300 MHz spectrometer with chemical shifts relative to tetramethylsilane (TMS, 0 ppm). UV-Vis spectra were collected on a Thermo Scientific GENESYS 20 Spectrophotometer. Cyclic voltammetry (CV) data were obtained with a BAS-CV-50W potentiostat/galvanostat using an Ag/AgCl reference electrode, a Pt wire counter electrode, and a Pt foil working electrode in 0.1 M tetrabutylammonium hexafluorophosphate in dry acetonitrile at a scan rate of 50 mV s^{-1}. Ferrocene was used as a reference, which has a highest occupied molecular orbital (HOMO) of −4.8 eV.[57] A Bruker D8 Advance powder diffractometer with standard Bragg–Bretano geometry using Cu Kα radiation ($\lambda = 1.5418$ Å) was used to collect the XRD patterns of polymer thin films (~100 nm) spin-coated on the dodecyltrichlorosilane (DTS)-modified SiO_2/Si substrates using polymer solutions in 1,1,2,2-tetrachloroethane (TCE). GPC measurements were performed on a Waters SEC system in chlorobenzene at 40 °C. A TGA Q500 instrument (TA Instruments) was used to conduct the thermogravimetry analysis (TGA) at a heating rate of 10 °C min^{-1} under nitrogen. AFM images were recorded on polymer thin films on DTS-modified SiO_2/Si substrates using a Dimension 3100 scanning probe microscope.

OTFT fabrication and characterization

A top-gate, bottom-contact OTFT structure was adopted for evaluating **P1** and **P2**. A heavily n-doped Si/SiO_2 wafer was used as the substrate. The source/drain electrode pairs were deposited using conventional photolithography to obtain the defined device dimensions with a channel length (L) of 30 μm and a channel width (W) of 1 mm. The substrate was cleaned using an ultrasonic bath with de-ionized (DI) water, and rinsed with acetone and isopropanol. Polymer films with a thickness of ~30–50 nm were deposited on the substrate by spin-coating a polymer solution in TCE (10 mg mL^{-1}) at 1500 rpm for 50 s and subsequently annealed at 100, 150 or 200 °C for 10 min. A CYTOP layer (~500 nm) was then spin-coated as the gate dielectric, and then dried at 100 °C on a hotplate for 30 min before depositing the Al gate electrode (~70 nm). All the devices were characterized in air in the absence of light using an Agilent 4155C Semiconductor Analyzer. Carrier mobility was calculated in the saturation regime according to the following equation:

$$I_D = \left(\frac{WC_i}{2L}\right)\mu(V_G - V_T)^2$$

where I_D is the drain current, μ is the charge carrier mobility, C_i is the capacitance per unit area of the insulator determined from a metal-insulator-metal structure (CYTOP, 500 nm, C_i = 3.2 nF cm^{-2}), V_G is the gate voltage, respectively.

Synthesis

6,6′-Dibromo-[2,2′-biindolinylidene]-3,3′-dione (1).[46] 4-Bromo-2-nitrobenzaldehyde (2 g, 8.7 mmol) was dissolved in acetone (90 mL) and water (100 mL) was added slowly. A 2 N aqueous NaOH solution was added dropwise to adjust the pH to 10. The suspension was then stirred overnight. Filtration gave a dark purple solid, which was washed with excess acetone and water. The resulting solid was dried *in vacuo* to give the product. Yield: 1.32 g (72.1%).

6,6′-Dibromo-1,1′-bis(2-hexyldecanoyl)-[2,2′-biindolinylidene]-3,3′-dione (2a). Compound **1** (0.672 g, 1.6 mmol) was dissolved in anhydrous *N*-methyl-2-pyrrolidone (NMP) (20 mL) at room temperature. Then sodium hydride (0.154 g, 6.4 mmol) was added and the mixture was stirred for 2 h. 2-Hexyldecanoyl chloride (1.319 g, 4.8 mmol) was added to the reaction mixture. After stirring for 24 h at room temperature, the reaction mixture was poured into de-ionized (DI) water, and extracted with ethyl acetate three times. The organic layer was washed with brine and DI water to remove NMP. The combined organic layer was dried over anhydrous sodium sulfate and filtered. After evaporating the solvent, the residue was purified by column chromatography on silica gel with toluene as an eluent to give the title compound as a dark purple solid. Yield: 0.491 g (34.2%). ^{1}H NMR (300 MHz, $CDCl_3$) δ 8.43 (s, 2H), 7.60 (d, J = 8.1 Hz, 2H), 7.39 (dd, J = 8.1, 1.3 Hz, 2H), 3.10–2.97 (m, 2H), 0.84 (t, J = 6.9 Hz, 12H). ^{13}C NMR (75 MHz, $CDCl_3$) δ 182.64, 150.03, 132.39, 128.26, 125.17, 119.80, 43.85, 31.79, 29.77, 29.41, 22.62, 14.06, 13.96.

6,6′-Dibromo-1,1′-bis(2-octyldodecanoyl)-[2,2′-biindolinylidene]-3,3′-dione (2b). Compound **2b** was synthesized following a similar procedure as that for the synthesis of **2a**, except for using 2-octyldodecanoyl chloride instead of 2-hexyldecanoyl chloride. Yield: 0.984 g (39.0%). ^{1}H NMR (300 MHz, $CDCl_3$) δ 8.43 (s, 2H), 7.60 (d, J = 8.1 Hz, 2H), 7.38 (dd, J = 8.1, 1.4 Hz, 2H), 3.11–2.96 (m, 2H), 0.87 (t, J = 7.5 Hz, 12H). ^{13}C NMR (75 MHz, $CDCl_3$) δ ^{13}C NMR (75 MHz, $CDCl_3$) δ 182.53, 149.93, 132.30, 128.18, 125.10, 119.70, 43.72, 31.78, 29.67, 29.47, 29.22, 22.56, 22.51, 13.98, 13.94.

Synthesis of P1

To a 25 mL dry flask was added **2a** (0.360 g, 0.401 mmol), 5,5′-bis(trimethylstannyl)bithiophene (0.197 g, 0.401 mmol) and tri(*o*-totyl)phosphine (9.8 mg, 0.0321 mmol). After degassing and refilling with argon 3 times, anhydrous chlorobenzene (8 mL) and tris(dibenzylideneacetone)-dipalladium (7.3 mg, 0.008 mmol) were added under an argon atmosphere. The mixture was stirred for 60 h at 90 °C. After being cooled to room temperature, the reaction mixture was poured into methanol and stirred for 0.5 h. The precipitated solid was collected by filtration and subjected to Soxhlet extraction with acetone, hexane, chloroform, and then the remaining polymer was heated in TCE at 130 °C and filtered after cooling. Very little polymer was dissolved in chloroform. The yield of the polymer dissolved in TCE was 52.4 mg (15.0%). The remaining polymer is insoluble.

Synthesis of P2

P2 was synthesized using **2b** (0.352 g, 0.349 mmol) and 5,5′-bis(trimethylstannyl)bithiophene (0.172 g, 0.349 mmol), following a similar procedure as that for the synthesis of **P1**. Yield: 49.1 mg (12.6%) from the chloroform extraction, 228.2 mg (58.7%) from the TCE extraction. The remaining polymer is insoluble.

Conclusions

We reported two new donor–acceptor polymers using indigo as the electron acceptor and bithiophene as the electron donor. Acyl groups, 2-hexldecanoyl (for polymer **P1**) and 2-octyldodecanoyl (for polymer **P2**), were used as the side chains to render these polymers soluble in organic solvents. The strong electron-withdrawing capability of the indigo moiety was manifested by the low-lying HOMO/LUMO levels, −5.69 eV/−4.00 eV for **P1** and −5.78 eV/−4.02 eV for **P2**. Due to the strong intramolecular D-A charge transfer, rather low band gaps (~1.7 eV) were observed for both polymers. The acyl side chains were found to cause serious twisting of the polymer backbone. These side chains are thermally labile and start to decompose at 160 °C for **P1** and 220 °C for **P2**. Thermal annealing led to notable red shifts of the absorption spectra, originating from the formation of more coplanar backbone structures. **P1** and **P2** showed characteristic electron transport performance in OTFTs with electron mobilities of up to 6.6 × 10^{-4} cm^2 V^{-1} s^{-1} and 1.1 × 10^{-3} cm^2 V^{-1} s^{-1}, respectively. The lower than expected field effect performance of these polymers in comparison to their counterpart isoindigo polymers was considered to be due to the backbone twisting and the presence of *cis*-indigo units that are undesirable for extended delocalization of electrons. Work on exploring other types of side chains to minimize the backbone twisting and the existence of *cis*-isomers to improve the charge transport performance of this new class of polymers is under way.

Acknowledgements

The authors thank the Natural Sciences and Engineering Research Council (NSERC) of Canada for financial support (Discovery Grants) of this research, and Dr Jianfu Ding at the National Research Council Canada (NRC) for the GPC measurements. The authors also thank Angstrom Engineering Inc. for providing the thermal deposition system for the fabrication of the OTFT devices.

Notes and references

1 C. Guo, W. Hong, H. Aziz and Y. Li, *Reviews in Advanced Sciences and Engineering*, 2012, **1**, 200–224.

2 Y. Li, P. Sonar, L. Murphy and W. Hong, *Energy Environ. Sci.*, 2013, **6**, 1684–1710.
3 A. Mishra, C.-Q. Ma and P. Bäuerle, *Chem. Rev.*, 2009, **109**, 1141–1276.
4 J. Chen and Y. Cao, *Acc. Chem. Res.*, 2009, **42**, 1709–1718.
5 R. S. Kularatne, H. D. Magurudeniya, P. Sista, M. C. Biewer and M. C. Stefan, *J. Polym. Sci., Part A: Polym. Chem.*, 2013, **51**, 743–768.
6 E. Bundgaard and F. C. Krebs, *Sol. Energy Mater. Sol. Cells*, 2007, **91**, 954–985.
7 R. Kroon, M. Lenes, J. C. Hummelen, P. W. M. Blom and B. de Boer, *Polym. Rev.*, 2008, **48**, 531–582.
8 A. Facchetti, *Chem. Mater.*, 2010, **23**, 733–758.
9 Y.-J. Cheng, S.-H. Yang and C.-S. Hsu, *Chem. Rev.*, 2009, **109**, 5868–5923.
10 J. W. Rumer, S.-Y. Dai, M. Levick, Y. Kim, M.-B. Madec, R. S. Ashraf, Z. Huang, S. Rossbauer, B. Schroeder, L. Biniek, S. E. Watkins, T. D. Anthopoulos, R. A. J. Janssen, J. R. Durrant, D. J. Procter and I. McCulloch, *J. Mater. Chem. C*, 2013, **1**, 2711–2716.
11 M. S. Almeataq, H. Yi, S. Al-Faifi, A. A. B. Alghamdi, A. Iraqi, N. W. Scarratt, T. Wang and D. G. Lidzey, *Chem. Commun.*, 2013, **49**, 2252–2254.
12 H. Bronstein, J. M. Frost, A. Hadipour, Y. Kim, C. B. Nielsen, R. S. Ashraf, B. P. Rand, S. Watkins and I. McCulloch, *Chem. Mater.*, 2013, **25**, 277–285.
13 I. Meager, R. S. Ashraf, S. Rossbauer, H. Bronstein, J. E. Donaghey, J. Marshall, B. C. Schroeder, M. Heeney, T. D. Anthopoulos and I. McCulloch, *Macromolecules*, 2013, **46**, 5961–5967.
14 J. Hou, M.-H. Park, S. Zhang, Y. Yao, L.-M. Chen, J.-H. Li and Y. Yang, *Macromolecules*, 2008, **41**, 6012–6018.
15 A. A. B. Alghamdi, D. C. Watters, H. Yi, S. Al-Faifi, M. S. Almeataq, D. Coles, J. Kingsley, D. G. Lidzey and A. Iraqi, *J. Mater. Chem. A*, 2013, **1**, 5165–5171.
16 I. Osaka, G. Sauve, R. Zhang, T. Kowalewski and R. D. McCullough, *Adv. Mater.*, 2007, **19**, 4160–4165.
17 Y. Li, S. P. Singh and P. Sonar, *Adv. Mater.*, 2010, **22**, 4862–4866.
18 Y. Zhu, R. D. Champion and S. A. Jenekhe, *Macromolecules*, 2006, **39**, 8712–8719.
19 B. Sun, W. Hong, H. Aziz, N. M. Abukhdeir and Y. Li, *J. Mater. Chem. C*, 2013, **1**, 4423–4426.
20 P. Sonar, T. R. B. Foong, S. P. Singh, Y. Li and A. Dodabalapur, *Chem. Commun.*, 2012, **48**, 8383–8385.
21 Y. Li, P. Sonar, S. P. Singh, W. Zeng and M. S. Soh, *J. Mater. Chem.*, 2011, **21**, 10829–10835.
22 Y. Li, P. Sonar, S. P. Singh, M. S. Soh, M. M. van and J. Tan, *J. Am. Chem. Soc.*, 2011, **133**, 2198–2204.
23 P. Sonar, S. P. Singh, Y. Li, M. S. Soh and A. Dodabalapur, *Adv. Mater.*, 2010, **22**, 5409–5413.
24 T. Lei, Y. Cao, Y. Fan, C.-J. Liu, S.-C. Yuan and J. Pei, *J. Am. Chem. Soc.*, 2011, **133**, 6099–6101.
25 J. Mei, D. H. Kim, A. L. Ayzner, M. F. Toney and Z. Bao, *J. Am. Chem. Soc.*, 2011, **133**, 20130–20133.
26 T. Lei, J.-H. Dou, Z.-J. Ma, C.-H. Yao, C.-J. Liu, J.-Y. Wang and J. Pei, *J. Am. Chem. Soc.*, 2012, **134**, 20025–20028.
27 T. Lei, J.-H. Dou and J. Pei, *Adv. Mater.*, 2012, **24**, 6457–6461.
28 E. D. Głowacki, G. Voss, L. Leonat, M. Irimia-Vladu, S. Bauer and N. S. Sariciftci, *Isr. J. Chem.*, 2012, **52**, 540–551.
29 P. E. McGovern and R. H. Michel, *Acc. Chem. Res.*, 1990, **23**, 152–158.
30 G. Sandberg, *Indigo Textiles: Technique and History*, Black, 1989.
31 R. Robinson, *J. Soc. Dyers Colour.*, 1921, **37**, 77–81.
32 J. Weinstein and G. M. Wyman, *J. Am. Chem. Soc.*, 1956, **78**, 2387–2390.
33 W. Lüttke and M. Klessinger, *Chem. Ber.*, 1964, **97**, 2342–2357.
34 M. Klessinger and W. Lüttke, *Chem. Ber.*, 1966, **99**, 2136–2145.
35 N. Yasarawan and J. S. van Duijneveldt, *Langmuir*, 2008, **24**, 7184–7192.
36 M. M. Sousa, C. Miguel, I. Rodrigues, A. J. Parola, F. Pina, J. S. Seixas de Melo and M. J. Melo, *Photochem. Photobiol. Sci.*, 2008, **7**, 1353–1359.
37 P. W. Sadler, *Spectrochim. Acta*, 1960, **16**, 1094–1099.
38 G. P. R. Haucke, *Photophysikalische Chemie indigoider Farbstoffe*, Deutsche Akademie d. Naturforscher Leopoldina, Barth, in Komm, Halle (Saale), Leipzig, 1978.
39 E. Wille and W. Lüttke, *Chem. Ber.*, 1973, **106**, 3240–3257.
40 E. A. Perpète, J. Preat, J.-M. André and D. Jacquemin, *J. Mater. Chem. A*, 2006, **110**, 5629–5635.
41 M. Irimia-Vladu, E. D. Głowacki, P. A. Troshin, G. Schwabegger, L. Leonat, D. K. Susarova, O. Krystal, M. Ullah, Y. Kanbur, M. A. Bodea, V. F. Razumov, H. Sitter, S. Bauer and N. S. Sariciftci, *Adv. Mater.*, 2012, **24**, 375–380.
42 E. D. Glowacki, L. Leonat, G. Voss, M.-A. Bodea, Z. Bozkurt, A. M. Ramil, M. Irimia-Vladu, S. Bauer and N. S. Sariciftci, *AIP Adv.*, 2011, **1**, 042132–042136.
43 Y. Kanbur, M. Irimia-Vladu, E. D. Głowacki, G. Voss, M. Baumgartner, G. Schwabegger, L. Leonat, M. Ullah, H. Sarica, S. Erten-Ela, R. Schwödiauer, H. Sitter, Z. Küçükyavuz, S. Bauer and N. S. Sariciftci, *Org. Electron.*, 2012, **13**, 919–924.
44 H. Kojima and T. Mori, *Chem. Lett.*, 2013, **42**, 68–70.
45 R. A. Marcus, *Rev. Mod. Phys.*, 1993, **65**, 599–610.
46 P. Imming, I. Imhof and M. Zentgraf, *Synth. Commun.*, 2001, **31**, 3721–3727.
47 K. Urano, T. Ohno, K. Tomono and K. Miyamura, *Bull. Chem. Soc. Jpn.*, 2013, **86**, 159–165.
48 B. Sun, W. Hong, H. Aziz and Y. Li, *J. Mater. Chem.*, 2012, **22**, 18950–18955.
49 J.-i. Setsune, H. Wakemoto, T. Matsueda, T. Matsuura, H. Tajima, T. Kitao, S. Ishihara and R. Yamamoto, *J. Chem. Soc., Perkin Trans. 1*, 1984, 2305–2309.
50 G. R. Seely and E. R. Shaw, *J. Photochem.*, 1984, **24**, 383–393.
51 Æ. Frisch, *Gaussian 09W Reference*, Gaussian, Inc., Wallingford, CT, 2009.
52 M. J. Frisch, *et al.*, *Gaussian 09*, 2009, see ESI† for the full citation.
53 Z. Ma, E. Wang, M. E. Jarvid, P. Henriksson, O. Inganas, F. Zhang and M. R. Andersson, *J. Mater. Chem.*, 2012, **22**, 2306–2314.

54 M. S. Chen, J. R. Niskala, D. A. Unruh, C. K. Chu, O. P. Lee and J. M. J. Frechet, *Chem. Mater.*, 2013, **25**, 4088–4096.
55 P. Friedländer, S. Bruckner and G. Deutsch, *Justus Liebigs Ann. Chem.*, 1912, **388**, 23–49.
56 Y. Sueishi, K. Ohtani and N. Nishimura, *Bull. Chem. Soc. Jpn.*, 1985, **58**, 810–814.
57 B. W. D'Andrade, S. Datta, S. R. Forrest, P. Djurovich, E. Polikarpov and M. E. Thompson, *Org. Electron.*, 2005, **6**, 11–20.
58 H. Sirringhaus, P. J. Brown, R. H. Friend, M. M. Nielsen, K. Bechgaard, B. M. W. Langeveld-Voss, A. J. H. Spiering, R. A. J. Janssen, E. W. Meijer, P. Herwig and D. M. de Leeuw, *Nature*, 1999, **401**, 685–688.
59 B. S. Ong, Y. Wu, Y. Li, P. Liu and H. Pan, *Chem.–Eur. J.*, 2008, **14**, 4766–4778.
60 S. Braun, W. R. Salaneck and M. Fahlman, *Adv. Mater.*, 2009, **21**, 1450–1472.
61 A. Wan, J. Hwang, F. Amy and A. Kahn, *Org. Electron.*, 2005, **6**, 47–54.